

Goldilocks Effect of a Distal Substituent on Living Ziegler–Natta Polymerization Activity and Stereoselectivity within a Class of Zirconium Amidinate-Based Initiators

Yonghui Zhang, Erin K. Reeder, Richard J. Keaton, and Lawrence R. Sita*

Department of Chemistry and Biochemistry, University of Maryland,
College Park, Maryland 20742

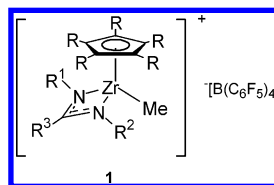
Received March 5, 2004

A new series of cationic zirconium amidinates, $[(\eta^5\text{-C}_5\text{Me}_5)\text{ZrMe}\{\text{N}(\text{Et})\text{C}(\text{R}^3)\text{N}(\text{tBu})\}]\text{[B(C}_6\text{F}_5)_4]$ ($\text{R}^3 = \text{Me, H, Ph, and tBu}$) (**1a–d**), were synthesized and their ability to function as initiators for the stereoselective living Ziegler–Natta polymerization of 1-hexene evaluated. Whereas **1a** is highly active for the isospecific living polymerization of 1-hexene as previously reported, polymerizations conducted with **1b** and **1c** both display a significant loss of stereocontrol, and in the case of **1b**, the polymerization is no longer living. Further, **1d** was found to be inactive for polymerization. The Goldilocks effect observed for the distal R^3 substituent in this series, i.e., **1b** “too small”, **1c** “too large”, **1a** “just right”, appears to be steric in origin. Solution and solid state structural studies suggest, however, that two different mechanisms are most likely operative for the loss of stereocontrol observed for **1b** and **1c**: a low barrier to metal-centered epimerization in the case of **1b** and a lack of steric discrimination at the metal center for olefin binding in the case of **1c**.

Introduction

Since the first important discovery by Doi and co-workers¹ of a well-defined metal complex that could serve as a homogeneous initiator for the living Ziegler–Natta polymerization of α -olefins below -65°C , the past decade has witnessed the successful demonstration of this same process by a small number of other nonmetallocene-based initiators that can operate at much higher temperatures, and in some cases, with a high degree of stereocontrol.^{2–9} With this success, it has

naturally been of interest to probe the steric and electronic factors that govern both the reactivity and stereoselectivity displayed by these various classes of initiators through manipulation of their ligand frameworks. In this regard, we originally reported that cationic zirconium amidinates of the general structure of **1** are capable of serving as highly active initiators



for the living polymerization of α -olefins and nonconjugated dienes.⁷ Further, in the specific case where $\text{R}^1 = \text{Et}$, $\text{R}^2 = \text{tBu}$, and $\text{R}^3 = \text{R} = \text{Me}$ (**1a**), the polymerization of α -olefins proceeds in a stereospecific manner to provide isotactic polyolefins through propagation involving strict 1,2-olefin insertion.^{7a,b} Subsequent investigations of this living system have focused on delineating structure/activity/stereoselectivity relationships by varying components of the ligand sphere that are in close proximity to the presumed olefin binding site. Importantly, these studies have served to show how sensitive polymerization activity and stereoselectivity are to nonbonded steric interactions presented by the ligand environment to the approaching olefin substrate.

(1) (a) Doi, Y.; Ueki, S.; Keli, T. *Macromolecules* **1979**, *12*, 814–819. (b) Doi, Y.; Ueki, S.; Keli, T. *Makromol. Chem. Macromol. Chem. Phys.* **1979**, *180*, 1359–1361.

(2) For a recent review, see: Coates, G. W.; Hustad, P. D.; Reinartz, S. *Angew. Chem., Int. Ed.* **2002**, *41*, 2236–2257.

(3) (a) Brookhart, M.; DeSimone, J. M.; Grant, B. E.; Tanner, M. J. *Macromolecules* **1995**, *28*, 5378–5380. (b) Killian, C. M.; Tempel, D. J.; Johnson, L. K.; Brookhart, M. *J. Am. Chem. Soc.* **1996**, *118*, 11664–11665.

(4) Scollard, J. D.; McConville, D. H. *J. Am. Chem. Soc.* **1996**, *118*, 10008–10009.

(5) (a) Baumann, R.; Davis, W. M.; Schrock, R. R. *J. Am. Chem. Soc.* **1997**, *119*, 3830–3831. (b) Mehrkhodavandi, P.; Bonitatebus, P. J.; Schrock, R. R. *J. Am. Chem. Soc.* **2000**, *122*, 7481–7482. (c) Mehrkhodavandi, P.; Schrock, R. R. *J. Am. Chem. Soc.* **2001**, *123*, 10746–10747.

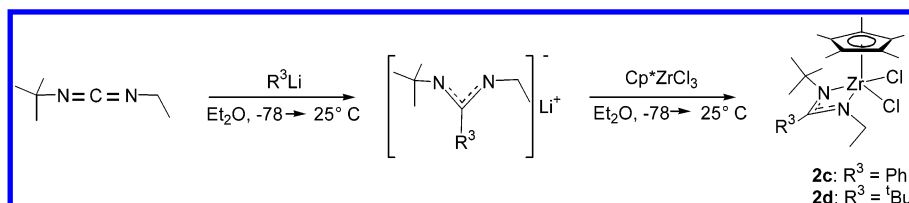
(6) (a) Matsui, S.; Tohi, Y.; Mitani, M.; Saito, J.; Makio, H.; Tanaka, H.; Nitabaru, M.; Nakano, T.; Fujita, T. *Chem. Lett.* **1999**, 1065–1066. (b) Saito, J.; Mitani, M.; Mohri, J.; Yoshida, Y.; Matsui, S.; Ishii, S.; Kojoh, S.; Kashiwa, N.; Fujita, T. *Angew. Chem., Int. Ed.* **2001**, *40*, 2918–2920. (c) Mitani, M.; Mohri, J.; Yoshida, Y.; Saito, J.; Ishii, S.; Tsuru, K.; Matsui, S.; Furuyama, R.; Nakano, T.; Tanaka, H.; Kojoh, S.; Matsugi, T.; Kashiwa, N.; Fujita, T. *J. Am. Chem. Soc.* **2002**, *124*, 3327–3336.

(7) (a) Jayaratne, K. C.; Sita, L. R. *J. Am. Chem. Soc.* **2000**, *122*, 958–959. (b) Jayaratne, K. C.; Keaton, R. J.; Henningsen, D. A.; Sita, L. R. *J. Am. Chem. Soc.* **2000**, *122*, 10490–10491. (c) Keaton, R. J.; Jayaratne, K. C.; Henningsen, D. A.; Koterwas, L. A.; Sita, L. R. *J. Am. Chem. Soc.* **2001**, *123*, 6197–6198. (d) Kissounko, D. A.; Fettingner, J. C.; Sita, L. R. *Inorg. Chim. Acta* **2003**, *345*, 121–129. (e) Zhang, Y.; Sita, L. R. *J. Chem. Soc., Chem. Commun.* **2003**, 2358–2359.

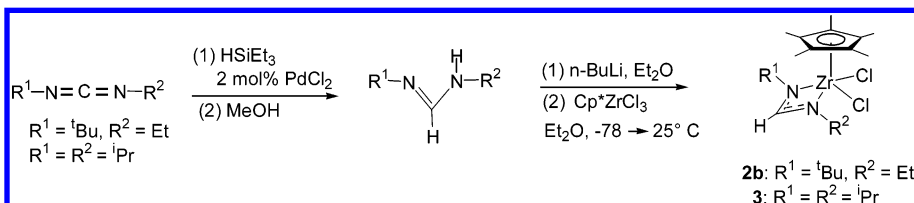
(8) (a) Tshuva, E. Y.; Goldberg, I.; Kol, M. *J. Am. Chem. Soc.* **2000**, *122*, 10706–10707. (b) Tshuva, E. Y.; Goldberg, I.; Kol, M.; Goldschmidt, Z. *J. Chem. Soc., Chem. Commun.* **2001**, 2120–2121.

(9) (a) Tian, J.; Coates, G. W. *Angew. Chem., Int. Ed.* **2000**, *39*, 3626–3629. (b) Tian, J.; Hustad, P. D.; Coates, G. W. *J. Am. Chem. Soc.* **2001**, *123*, 5134–5135.

Scheme 1



Scheme 2



To briefly summarize what has currently been mapped out, the larger steric bulk provided by the $\eta^5\text{-C}_5\text{Me}_5$ (Cp^*) vs the $\eta^5\text{-C}_5\text{H}_5$ (Cp) group (i.e., $\text{R} = \text{Me}$ and H in **1**, respectively) is critical for directing olefin stereoface selectivity, thereby providing a highly isotactic polymer microstructure ($mmmm \geq 99\%$) in the former case, but nearly atactic material in the latter.^{7c} Of greater surprise, however, was the observed sensitivity of activity and stereoselectivity to replacement of the N-Et group of the amidinate ligand in **1a** with $\text{N-CH}_2\text{X}$ substituents, where X varied in size from isopropyl to phenyl to *tert*-butyl.^{7d} More specifically, with a $\text{N-Et} \rightarrow \text{N-}^t\text{Bu}$ substitution, polymerization activity decreased dramatically, and a loss of stereocontrol was observed to provide a nearly atactic microstructure. In contrast, the $\text{N-Et} \rightarrow \text{N-CH}_2\text{Ph}$ substitution yielded an initiator that retained both the high activity and stereoselectivity displayed by **1a**. In both of these substitutions, the living character of the polymerization was also preserved. Finally, the $\text{N-Et} \rightarrow \text{N-CH}_2\text{CMe}_3$ substitution provided an inactive cationic complex, presumably due to substantial crowding about the metal center that prevents productive olefin binding.

With the high degree of sensitivity to proximal groups established for **1**, attention was next turned to determining what influence *distal* groups within the ligand environment might have on living character, activity, and stereoselectivity. In this report, the results of varying the steric bulk of the Me group in the amidinate fragment of **1a** (i.e., $\text{R}^3 = \text{Me}$ in **1**) are presented. More specifically, a comparison of living character, activity, and stereoselectivity in the Ziegler–Natta polymerization of 1-hexene for the $\text{R}^3 = \text{Me} \rightarrow \text{H}$, Me , Ph , and ^tBu replacements reveals how sensitive these parameters can also be to the influence of distal parts of the ligand environment. Perhaps more importantly, these observations show, once again, how difficult it is to “rationally” design an optimum initiator based on a new ligand from first principles.¹⁰

Results and Discussion

(a) Synthesis of $\text{Cp}^*\text{ZrCl}_2[\text{N}(\text{R}^1)\text{C}(\text{R}^3)\text{N}(\text{R}^2)]$ ($\text{R}^1 = \text{Et}$, $\text{R}^2 = ^t\text{Bu}$, $\text{R}^3 = \text{Me}$, H , Ph , ^tBu (2a–d**) and $\text{R}^1 = \text{R}^2 = ^i\text{Pr}$, $\text{R}^3 = \text{H}$ (**3**)).** Although a large number of derivatives of **1** have now been conveniently prepared in one step by utilizing carbodiimide insertion into a

Zr-C_{Me} bond of in situ generated Cp^*ZrMe_3 ,⁷ to vary the nature of the R^3 substituent, different synthetic strategies were employed to prepare compounds **2a–d** where $\text{R}^3 = \text{Me}$, H , Ph , and ^tBu , respectively. To begin, following the synthetic route to **2a** published previously,¹¹ compounds **2c** and **2d** were prepared by first generating the corresponding lithium amidinate salts through addition of the appropriate organolithium reagent to commercially available 1-*tert*-butyl-3-ethylcarbodiimide. As shown in Scheme 1, these lithium reagents were then used to produce **2c** and **2d** in high yield from Cp^*ZrCl_3 through standard procedures.

Synthesis of the formamidinate complex **2b** (i.e., $\text{R}^3 = \text{H}$) required a slightly different path. As shown in Scheme 2, the required lithium formamidinate was prepared through deprotonation of the corresponding amidine, which in turn was obtained through hydrosilylation of the carbodiimide followed by methanolysis of the silyl group according to the procedure of Ojima and co-workers.¹² Following the same procedure, the C_s -symmetric compound **3** was prepared as well since a greater range of structure/property relationships were of interest. In this regard, we have previously observed for **1a** that replacement of the $\text{R}^1 = \text{Et}$, $\text{R}^2 = ^t\text{Bu}$ combination by the $\text{R}^1 = \text{R}^2 = ^i\text{Pr}$ substituent pattern greatly attenuates polymerization activity, presumably due to a greater steric shielding of the metal center in the latter case.

Spectroscopic and chemical analyses were all consistent with the structures depicted for compounds **2a–d** and **3**. Importantly, ^1H NMR spectroscopy revealed that a low barrier for racemization of the metal center through amidinate ring-flipping¹³ exists for these compounds, regardless of the steric bulk of the distal amidinate substituent, such that this racemization proceeds readily at room temperature on the NMR time scale. This result is somewhat surprising in that we have previously determined that monoalkylation of **2a** provides chloro, alkyl complexes, such as **4** ($\text{X} = \text{Cl}$, R

(10) See also for instance: (a) Busico, V.; Van Axel Castelli, V.; Aprea, P.; Cipullo, R.; Segre, A.; Talarico, G.; Vacatello, M. *J. Am. Chem. Soc.* **2003**, *125*, 5451–5460. (b) Talarico, G.; Busico, V.; Cavallo, L. *J. Am. Chem. Soc.* **2003**, *125*, 7172–7173.

(11) Keaton, R. J.; Koterwas, L. A.; Fetting, J. C.; Sita, L. R. *J. Am. Chem. Soc.* **2002**, *124*, 5932–5933.

(12) Ojima, I.; Inaba, S. *J. Organomet. Chem.* **1977**, *140*, 97–111.

(13) (a) Sita, L. R.; Babcock, J. R. *Organometallics* **1998**, *17*, 5228–5230. (b) Koterwas, L. A.; Fetting, J. C.; Sita, L. R. *Organometallics* **1999**, *18*, 4183–4190.

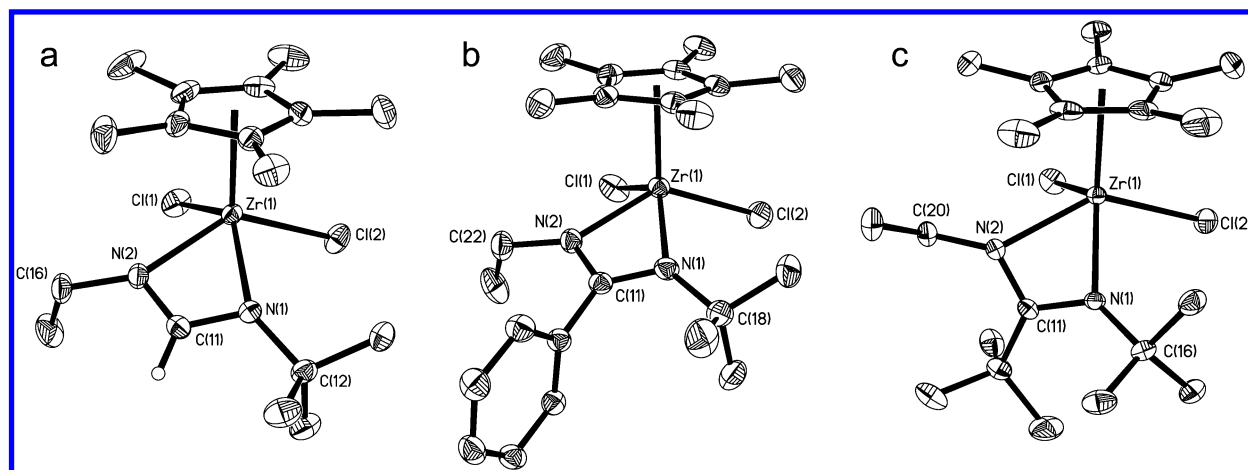


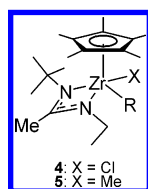
Figure 1. Molecular structures (30% thermal ellipsoids) of (a) **2b**, (b) **2c**, and (c) **2d**. Hydrogen atoms, except for that on C(11) of **2b** (drawn as a sphere of arbitrary size), have been removed for the sake of clarity.

Table 1. Selected Bond Lengths and Bond Angles for the Molecular Structures of **2b–d**, **6a**, **6b**, **6d**, and **1d**

	2b	2c	2d	6b	6a^a	6d	1d
bond lengths (Å)							
Zr(1)–N(1)	2.2446(11)	2.2645(2)	2.177(3)	2.3029(9)	2.265(2)	2.215(4)	2.123(3)
Zr(1)–N(2)	2.2218(17)	2.176(2)	2.278(3)	2.2770(9)	2.251(3)	2.333(4)	2.157(3)
N(1)–C(11)	1.327(2)	1.331(4)	1.3197(18)	1.3238(14)	1.332(4)	1.367(6)	1.349(4)
N(2)–C(11)	1.321(2)	1.334(4)	1.3268(19)	1.3219(15)	1.323(4)	1.320(6)	1.338(4)
bond angles (deg)							
N(1)–Zr(1)–N(2)	60.01(5)	59.60(9)	58.95(12)	58.94(3)	58.40(9)	57.50(13)	61.33(10)
Zr(1)–N(1)–C(11)	91.59(10)	92.20(17)	92.5(2)	89.86(6)	92.76(17)	93.4(3)	95.57(19)
Zr(1)–N(1)–C [†] _{Bu}	146.40(9)	140.6(2)	136.6(2)	147.30(7)	142.5(16)	135.1(3)	117.95(19)
C(11)–N(1)–C [†] _{Bu}	118.88(12)	125.4(2)	130.4(3)	118.01(9)	122(2)	128.5(4)	141.6(3)
Zr(1)–N(2)–C(11)	92.77(11)	96.13(17)	89.2(2)	91.03(6)	93.62(18)	89.5(3)	94.36(19)
Zr(1)–N(2)–C [†] _{Et}	145.64(16)	140.4(2)	131.4(2)	141.20(8)	136.4(17)	132.7(3)	136.3(2)
C(11)–N(2)–C [†] _{Et}	119.93(17)	123.3(3)	127.0(3)	117.65(10)	123.5(16)	126.5(4)	129.0(3)
N(1)–C(11)–N(2)	115.05(15)	111.9(2)	108.3(3)	116.79(10)	112.2(2)	109.2(4)	108.7(3)
Σθ _{N(1)} (deg) ^b	356.87	358.20	359.5	355.17	357.26	357.0	355.12
Σθ _{N(2)} (deg) ^c	358.34	359.83	347.6	349.88	353.52	348.7	359.66
φ (deg) ^d	7.8	3.8	34.7	18.6	18.3	33.6	3.1

^a From ref 19. ^b Sum of angles: Zr(1)–N(1)–C(11), Zr(1)–N(1)–C[†]_{Bu}, C(11)–N(1)–C[†]_{Bu}. ^c Sum of angles: Zr(1)–N(2)–C(11), Zr(1)–N(2)–C[†]_{Et}, C(11)–N(2)–C[†]_{Et}. ^d Angle between the mean planes defined by the following: Zr(1)–N(1)–C(11) and Zr(1)–N(2)–C(11).

= isobutyl), that are configurationally stable, even at elevated temperatures up to 80 °C, whereas dialkylation of **2a** provides dialkyl complexes, such as **5** (X = Me, R = isobutyl), that undergo metal-centered racemization even at subambient temperatures.^{11,14,15} On the basis of solid-state structures for different derivatives of **4** and **5**, we speculated that the greater electronegativity of



the chloro group results in a strengthening of zirconium–nitrogen bonding interactions that, in turn, raise the barrier to amidinate ring-flipping.¹⁶ Given that compounds **2a–d** and **3** possess two chloro substituents, it was naturally of interest to test this hypothesis further by obtaining solid-state structural information for them.

Figure 1 presents the molecular structures of compounds **2b–d** as obtained from single-crystal X-ray analysis; and Table 1 gives some selected bond lengths and bond angles. As anticipated, having two chloro groups on the zirconium center does indeed appear to reduce zirconium–nitrogen bonds further relative to either **4** or **5**. For example, in compound **2b**, the Zr–N distances are 2.2218(17) and 2.2446(11) Å, and in the structure of **3**, which has also been determined,¹⁷ they are 2.2159(12) and 2.2229(11) Å. In contrast, the corresponding Zr–N bond lengths in a chloro, isopropyl zirconium acetamidinate complex (i.e., X = Cl, R = ⁱPr in **4**) are 2.2419(11) and 2.2528(11) Å, while for a methyl, isopropyl derivative (i.e., X = Me, R = ⁱPr in **5**), these values are 2.2594(9) and 2.2809(9) Å.^{15,16} However, it is now clear that given the configurational instability of **2**, this reduction in Zr–N bond lengths relative to **4** and **5** is not sufficient by itself to provide a significant barrier to racemization. Accordingly, configurational stability is most likely determined by a subtle combination of both electronic and steric effects provided by the level of chloro vs alkyl substitution at the metal center. Regardless of the influence of these proximal substituents, it certainly does appear true that

(14) Zhang, Y.; Keaton, R. J.; Sita, L. R. *J. Am. Chem. Soc.* **2003**, *125*, 9062–9069.

(15) Zhang, Y.; Keaton, R. J.; Sita, L. R. *J. Am. Chem. Soc.* **2003**, *125*, 8746–8747.

(16) Harney, H. B.; Keaton, R. J.; Sita, L. R. Manuscript in preparation.

(17) Detailed information is provided in the Supporting Information.

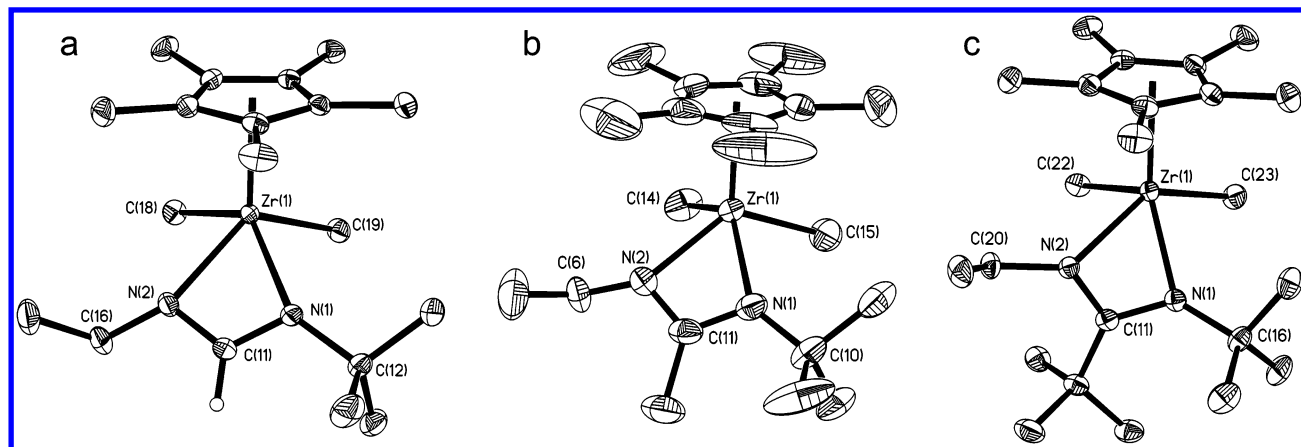


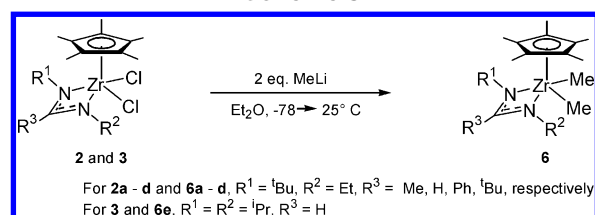
Figure 2. Molecular structures (30% thermal ellipsoids) of (a) **6b**, (b) **6a**, and (c) **6d**. Hydrogen atoms, except for that on C(11) of **6b** (drawn as a sphere of arbitrary size), have been removed for the sake of clarity.

the steric bulk of the distal amidinate substituent plays no or at best a very small role in controlling the barrier to racemization in **2**.

The strongest influence of distal effects within the series of **2b–d** can be seen in the value of the bond angles about the nitrogen atoms. Of greatest significance is the reduction in the Zr–N–C_{exo} bond angles as the steric bulk of the amidinate substituent increases in going from **2b** [146.40(9) and 145.64(16)°] to **2c** [140.6(2) and 140.4(2)°] to **2d** [136.6(2) and 131.4(2)°]. This reduction is accompanied by a concomitant increase in the C_{exo}–N–C(11) bond angles [cf. **2b**, 118.88(12)° and 119.93(17)°; **2c**, 125.4(2)° and 123.3(3)°; **2d**, 136.6(2)° and 131.4(2)°]. Thus, as a result of “buttressing” effects¹⁸ that arise with the increasing steric bulk of the C-amidinate substituent (i.e., R³ in **1**), the metal center becomes increasingly more shielded in the order **2b** < **2c** < **2d**. A final geometric perturbation of note is the extent of puckering of the four-membered amidinate ring as quantified by the angle between the two mean planes defined by Zr(1)–N(1)–C(11) and Zr(1)–N(2)–C(11). As can be seen in Table 1, the amidinate ring is nearly planar for compounds **2b** and **2c** (cf. 7.8° and 3.8°, respectively), whereas in compound **2d** it is significantly puckered (cf. ϕ = 34.7°). Closer inspection of the molecular structure of **2d**, including analysis of a space-filling representation, reveals that the strong nonbonded steric interactions prevent all three amidinate substituents from lying in the same plane. Oddly, however, it is the Zr–N bond distance involving the nitrogen with the N–Et substituent that is the longest, and it is this same nitrogen atom, N(2), that becomes significantly more pyramidalized than the one bearing the N–^tBu group (cf. $\Sigma\theta_{N(2)} = 347.6^\circ$ vs $\Sigma\theta_{N(1)} = 359.5^\circ$).

(b) Synthesis of Cp*ZrMe₂[N(R¹)C(R³)N(R²)] (R¹ = Et, R² = ^tBu, R³ = Me, H, Ph, ^tBu (6a–d**) and R¹ = R² = ⁱPr, R³ = H (**6e**)).** Following standard published procedures, methylation of **2a–d** and **3** with 2 equiv of methyl lithium proceeded smoothly in diethyl ether to provide the corresponding dimethyl derivatives **6a–e** in high yield according to Scheme 3. Once again, spectroscopic and chemical analyses were consistent

Scheme 3

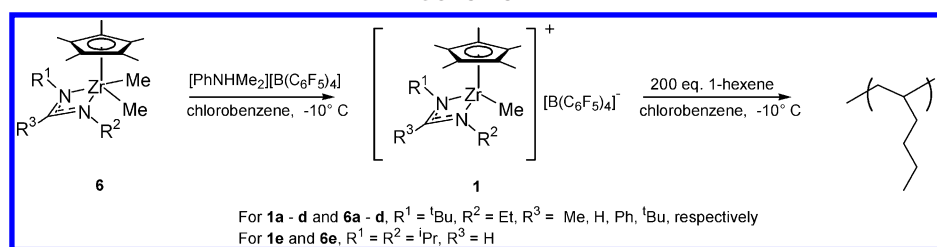


with the formulation of these compounds as presented, and in keeping with all other dialkyl derivatives prepared to date, **6a–e** were found to be configurationally unstable on the ¹H NMR time scale with respect to metal-centered racemization. Finally, to aid in the further development of structure/property relationships, the molecular structures of **6a**, **6b**, and **6d** were determined by single-crystal X-ray analysis and Figure 2 and Table 1 present the molecular structures and selected geometric parameters for these compounds, respectively.^{17,19} As expected, the Zr–N bond distances in these compounds are significantly longer than those in their corresponding dichloro derivatives [cf. 2.2446(11) and 2.2218(17) Å for **2b** vs 2.2770(9) and 2.3029(9) Å for **6b**]. With respect to the influence of the distal amidinate substituent, the trends observed previously for the angles about the nitrogen atoms are observed here as well. More specifically, as one goes from **6b** (R³ = H) to **6a** (R³ = Me) to **6d** (R³ = ^tBu), there is a steady reduction in the Zr–N–C_{exo} bond angles [cf. 147.30(7)° and 141.20(8)° for **6b**; 142.5(16)° and 136.4(17)° for **6a**; 135.1(3)° and 132.7(3)° for **6d**] and a steady increase in the C_{exo}–N–C(11) bond angle [cf. 118.01(9)° and 117.65(10)° for **6b**; 122(2)° and 123.50(16)° for **6a**; 128.5(4)° and 126.5(4)° for **6d**]. Thus, buttressing effects again serve to increasingly shield the metal center as the steric bulk of the distal R³ ligand increases. One surprising feature for some of these dimethyl structures, however, is that the amidinate fragment is much more nonplanar than in the corresponding dichloro analogues. For instance, the value of the angle, ϕ , is ~18.5° for both **6a** and **6b**, whereas both of the respective dichloro derivatives have nearly planar four-membered rings (vide supra). Given the similar sizes of chloro and methyl groups, it is possible that this geometric differ-

(18) For a discussion of similar buttressing effects in group 13 amidinate complexes, see: (a) Dagorne, S.; Jordan, R. F.; Young, V. G., Jr. *Organometallics* **1999**, *18*, 4619–4623. (b) Dagorne, S.; Guzei, I. A.; Coles, M. P.; Jordan, R. F. *J. Am. Chem. Soc.* **2000**, *122*, 274–289.

(19) Keaton, R. J.; Jayaratne, K. C.; Fetting, J. C.; Sita, L. R. *J. Am. Chem. Soc.* **2000**, *122*, 12909–12910.

Scheme 4

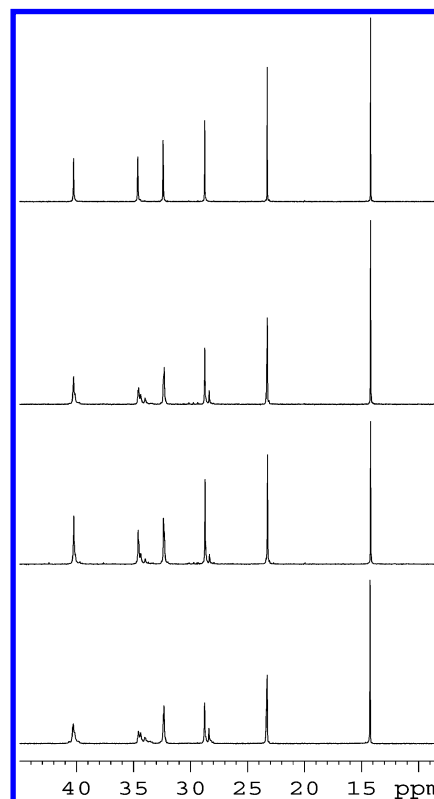
**Table 2. Data for Polymerization of 1-Hexene by **1a–e**^{a,b}**

initiator	yield (%)	M_n	M_w/M_n
1a	95	19 800	1.03
1b	45	20 100	1.59
1c	90	19 300	1.02
1d	no activity		
1e	98	25 100	1.23

^a Polymerizations were conducted for 2 h in chlorobenzene at $-10\text{ }^\circ\text{C}$, using 200 equiv of 1-hexene and $2.5\text{ }\mu\text{mol}$ of **6**. ^b M_n and M_w/M_n values were obtained from GPC and are reported relative to polystyrene standards.

ence between the two series is largely electronic in origin. On the other hand, the ϕ value of 33.6° for **6d** is quite similar to that found for **2d**, thus suggesting that strong nonbonded interactions between the amidinate substituents can override any electronic effects at the metal center.

(c) In Situ Generation of $[\text{Cp}^*\text{ZrMe}\{\text{N}(\text{R}^1)\text{C}(\text{R}^3)\text{N}(\text{R}^2)\}][\text{B}(\text{C}_6\text{F}_5)_4]$ and Polymerization Studies with 1-Hexene. Polymerizations of 200 equiv of 1-hexene were conducted according to Scheme 4 by generating the cationic initiators **1a–e** in chlorobenzene at $-10\text{ }^\circ\text{C}$ through reaction of the dimethyl precursors **6a–e** with 1 equiv of the borate, $[\text{PhNHMe}_2][\text{B}(\text{C}_6\text{F}_5)_4]$. After a fixed polymerization time of 2 h, the polymerizations were quenched and the poly(1-hexene) material isolated and purified by precipitation. ^1H NMR was then used to assess the presence of vinylic end groups that might arise from termination during propagation via β -hydride elimination, while ^{13}C NMR was used to determine the tacticity of the polymer microstructure. Table 2 and Figure 3 present relevant data obtained from these polymerization studies. To begin, both the M_n and M_w/M_n values recorded for poly(1-hexene) obtained from **1a** are similar to previously published results⁷ and they are in agreement with those expected for a living polymerization proceeding with quantitative conversion of the monomer. Further, the ^{13}C NMR spectrum shown in Figure 3 confirms that the microstructure of this material is perfectly isotactic. For initiator **1c**, similar M_n , M_w/M_n , and yield of polymer were obtained; however, a ^{13}C NMR spectrum now revealed that a significant loss of stereocontrol had occurred to provide a microstructure that is only slightly iso-rich as presented in Figure 3. On the other hand, polymerizations with **1b** proceeded in poor yield for the same period of time and the polymerization was not living as indicated by the significantly larger polydispersity that is observed (i.e., $M_w/M_n = 1.58$). The ^{13}C NMR spectrum of the poly(1-hexene) obtained from **1b** shown in Figure 3 reveals it to be more iso-rich than that obtained from **1c**, but a loss of stereocontrol relative to **1a** is definitely seen. For the C_s -symmetric derivative **1e**, poly(1-hexene) was obtained in high yield and with a narrower polydispersity

**Figure 3.** $^{13}\text{C}\{^1\text{H}\}$ NMR (100 MHz, chloroform-*d*, $25\text{ }^\circ\text{C}$) spectra of poly(1-hexene) obtained from, top to bottom, **1a**, **1c**, **1b**, and **1e**.

sity (cf. $M_w/M_n = 1.23$); however, the higher M_n and M_w/M_n values relative to **1a** still suggest that this polymerization was not strictly living in character. The ^{13}C NMR spectrum of the polymer obtained from **1e** was expectedly much more nearly atactic as revealed by Figure 3 with the small degree of isoselectivity possibly arising from chain-end control.^{7c} Finally, the cationic complex **1d** displayed no catalytic activity even at room temperature presumably due to a large degree of steric crowding about the metal center that prevents productive olefin binding.

The polymerization data shown in Table 2 and Figure 3 present a clear example of a “Goldilocks” effect for the relationship between the steric bulk of the R^3 group and several key parameters for 1-hexene polymerization by the initiators **1a–d**, including activity, stereocontrol, and living character. Restating this in more general terms, it would appear that while $\text{R}^3 = \text{H}$ (**1b**) is “too small” and $\text{R}^3 = \text{Ph}$ (**1c**) and ${}^i\text{Bu}$ (**1d**) are “too large”, $\text{R}^3 = \text{Me}$ (**1a**) is “just right”. A closer look at the solution structures of **1a–d** and the solid-state structure of **1d** shed more light on the steric origins of this Goldilocks effect of the distal amidinate substituent. To begin, we have previously demonstrated through the use of vari-

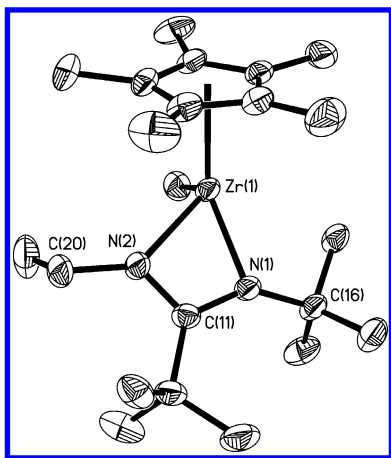


Figure 4. Molecular structures (30% thermal ellipsoids) of **1d**. Hydrogen atoms and the borate counterion have been removed for the sake of clarity.

able-temperature NMR spectroscopy that while neutral **6a** undergoes facile metal-centered racemization even at low temperatures, cationic **1a** is configurationally stable up to temperatures of at least 25 °C.^{14,20} Using this same technique, it was surprisingly discovered that initiator **1b** is *not* configurationally stable at -10 °C, whereas both **1c** and **1d** are. Thus, it becomes more obvious that the buttressing effects initiated by the R³ amidinate group that were observed in the solid-structures of neutral **2** and **6** are playing a critical role in controlling the barrier to amidinate ring-flipping in cationic **1**. In the case of **1b**, the rate of epimerization of the metal center of the propagating center must be close to the rate of propagation, which then gives rise to the partial loss of stereocontrol observed for this initiator. In the case of **1c**, we have previously noted that to obtain a high degree of stereocontrol in the polymerization of 1-hexene, there must be sufficient steric discrimination being presented to the incoming monomer by the two N-substituents of the amidinate group (vide supra).^{7d} It would thus appear likely that this steric discrimination is lost in the case where R³ = Ph due to the buttressing effects that serve to push both of the N-substituents forward. Importantly, this analysis concludes that the steric origin of decreased stereocontrol observed for **1c** is different than that observed for **1b**. Finally, it was of interest to determine at what point does this buttressing effect of the amidinate group prevent productive olefin binding, and to this end, the solid-state structure of **1d** was obtained. Figure 4 presents the molecular structure of **1d**, and Table 1 gives some selected bond lengths and bond angles. To begin, **1d** was found to be monomeric in the solid state as opposed to the dimeric dication structure obtained for **1a**,¹⁹ and this observation already suggests that significant steric crowding must be present about the metal to prevent such dimerization from occurring. By now looking at the same set of structural parameters discussed previously for **6d**, some notable differences can be seen in the molecular structure of cationic **1d**, and in particular, in the geometry of the amidinate fragment. More specifically, although the Zr–N bonds of **1d** are shorter than those in **6d**, the amidinate four-

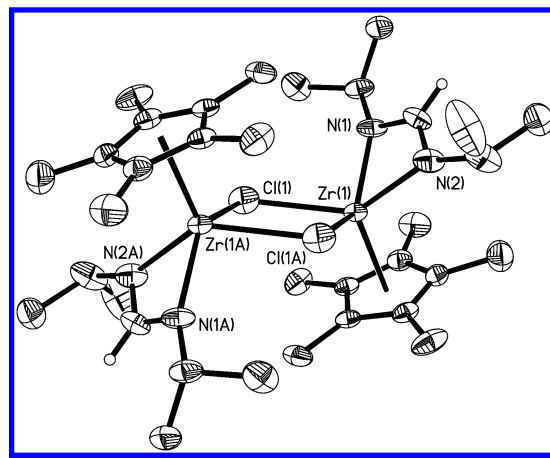


Figure 5. Molecular structures (30% thermal ellipsoids) of **7**. Hydrogen atoms, except those on C(11) and C(11A), and the borate counterions have been removed for the sake of clarity.¹⁷

membered ring is now nearly planar (cf. a ϕ value of 3.1° for **1d** vs 33.6° for **6d**) and both of the nitrogen atoms are more trigonal coplanar. Further, the Zr–N–C_{exo} and C_{exo}–N–C(11) bond angles of 117.94(19)° and 141.6(3)° in **1d** are opposite in magnitude to the corresponding values seen for **6d**. Thus, altogether, these differences suggest that formation of the cationic species **1d** through demethylation of **6d** can be likened to releasing a spring under compression in which the steric interactions pent up in **6d** are removed by allowing the N-^tBu substituent to swing into the position previously occupied by the departing methyl group. It is then likely that this structural displacement of the N-^tBu group is responsible for preventing the remaining methyl group from exiting the olefin binding pocket, which is presumed to be on the N-Et side of the amidinate group.

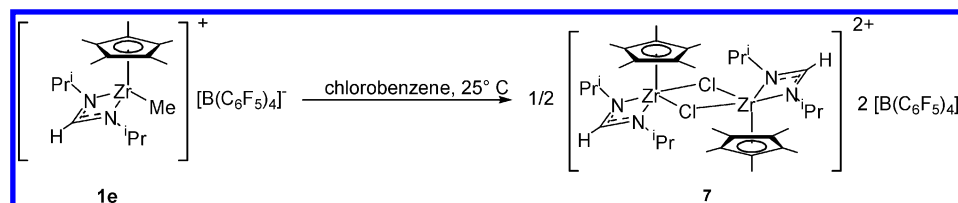
One answer to the question of why polymerizations using the formamidinate initiators **1b** and **1e** are not living comes from analysis of the orange-red crystalline material obtained from chlorobenzene solutions of **1e** left for a few hours at 25 °C. As Figure 5 reveals, this compound proved to be the μ -Cl dimeric dication **7** that presumably arises from chloride abstraction from the solvent according to Scheme 5, although the ultimate fate of the methyl group is not presently known. Similar μ -chloro dicationic dizirconium species have been observed by Green and co-workers²¹ and Collins and co-workers²² from demethylations of other zirconium complexes. We have also obtained the analogous compound, {Cp*Zr(μ -Cl)[N(^tBu)C(Me)N(Et)]₂}[B(C₆F₅)₄]₂ (**8**), from chlorobenzene solutions of **1a**; however, in this case, much longer reaction times were required. If this difference in reactivity is associated with a lesser degree of steric crowding about the metal center in **1e** than in **1a**, then it is safe to assume that given the even greater metal accessibility of **1b**, propagating species derived from it will be even more highly susceptible to reaction with the solvent. Thus, the increase in living character in the order **1b** < **1e** < **1a** is readily explained.

(21) Gomez, R.; Green, M. L. H.; Haggitt, J. L. *J. Chem. Soc., Dalton Trans.* **1996**, 939–946.

(22) Vollmerhaus, R.; Rahim, M.; Tomaszewski, R.; Xin, S.; Taylor, N. J.; Collins, S. *Organometallics* **2000**, *19*, 2161–2169.

(20) Jayaratne, K. C.; Sita, L. R. *J. Am. Chem. Soc.* **2001**, *123*, 10754–10755.

Scheme 5



Concluding Remarks

The results described herein demonstrate how sensitive key parameters for the homogeneous metal-catalyzed Ziegler–Natta polymerization of α -olefins, including activity, stereoselectivity, and living character, can be to the steric bulk of distal parts of the ligand sphere that are transmitted to the metal center of the propagating species through buttressing effects. In the examples shown, a distinct Goldilocks effect was observed where a fine balance between nonliving character and no activity is controlled by the steric bulk of the distal amidinate substituent. Importantly, with respect to the loss of stereocontrol observed for **1b** and **1c**, it was determined that two different mechanisms can be operative depending upon the steric bulk of the distal amidinate substituent: a low barrier to metal-centered epimerization in the case of **1b** and a lack of steric discrimination at the metal center for olefin binding in the case of **1c**. Taken together, the present study once again points out the difficulties in obtaining a highly active initiator for living and/or stereoselective Ziegler–Natta polymerization from first principles based on a new ligand design, and only through fortuitous circumstance might one achieve success the first time, or after only a few iterative modifications of the ligand framework. In this regard, the introduction of high throughput screening strategies that can more easily explore a greater range of ligand structural diversity in a shorter period of time has much to offer.²³

Experimental Section

All manipulations were performed under an inert atmosphere of dinitrogen, using standard Schlenk techniques or a Vacuum Atmospheres glovebox. Dry, oxygen-free solvents were employed throughout. Diethyl ether (Et_2O) and pentane were distilled from NaK. MeLi (in Et_2O), PhLi (in cyclopentane/ Et_2O), and tBuLi (in pentane) were purchased from Aldrich and used as received. Cp^*ZrCl_3 was obtained from Strem and $[\text{PhNHMe}_2][\text{B}(\text{C}_6\text{F}_5)_4]$ was obtained from Boulder Scientific. Compounds **2a** and **6a** were prepared according to previously reported procedures.^{7,11} Chlorobenzene was distilled from calcium hydride and 1-hexene was vacuum transferred from NaK prior to being used for polymerizations. GPC analyses were performed with a Waters GPC system equipped with a column oven and a differential refractometer both maintained at 40 °C and four columns (Waters Ultrastaygel 500 Å, Waters Styragel HR3, Waters Styragel HR4, and Shodex K-806M) also maintained at 40 °C. THF was used as the eluant at a flow rate of 1.1 mL/min. M_n and M_w/M_n values were obtained with the Waters GPC software and seven different polystyrene standards (Polymer Laboratories). For NMR, benzene- d_6 was vacuum transferred from NaK prior to use. ^1H NMR and $^{13}\text{C}\{^1\text{H}\}$ NMR spectra were recorded at 400 and 100 MHz, respectively, using chloroform- d or benzene- d_6 as the solvents.

$\text{tBuN}=\text{C}(\text{H})\text{-N}(\text{Et})\text{SiEt}_3$. A mixture of 10.1 g (80.0 mmol) of 1-*tert*-butyl-3-ethylcarbodiimide, 11.1 g (95.4 mmol) of triethylsilane, and 0.24 g (1.35 mmol) of PdCl_2 was sealed in a Schlenk tube and heated at 150 °C overnight. After the mixture was cooled to room temperature, the crude product was vacuum distilled at 85 °C (4 mmHg) to provide the desired material as a light yellow liquid (11.6 g, 61% yield). ^1H NMR (400 MHz, benzene- d_6 , 25 °C) δ 7.57 (s, 1H), 3.26 (q, $^3J = 6.8$ Hz, 2H), 1.28 (s, 9H), 1.18 (t, $^3J = 6.8$ Hz, 3H), 0.90 (t, $^3J = 7.6$ Hz, 9H), 0.59 (q, $^3J = 7.6$ Hz, 6H).

$\text{tBuN}=\text{C}(\text{H})\text{-NHtEt}$. To 11.6 g (47.8 mmol) of freshly distilled $\text{tBuN}=\text{C}(\text{H})\text{-NH}(\text{Et})\text{SiEt}_3$ was added 1.8 g (56 mmol) of methanol. After 1 h, vacuum distillation provided 5.0 g (81% yield) of the desired product as a colorless liquid. ^1H NMR (400 MHz, CDCl_3 , 25 °C) δ 7.40 (s, 1H), 3.16 (q, $^3J = 7.2$ Hz, 2H), 1.18 (s, 9H), 1.10 (t, $^3J = 7.2$ Hz, 3H).

Compound 2b. To a solution of 1.03 g (8.00 mmol) of $\text{tBuN}=\text{C}(\text{H})\text{-NH}(\text{Et})$ in 100 mL of Et_2O , cooled to –30 °C, was added 2.81 mL of *n*-BuLi (2.90 M in hexane, 8.16 mmol) via a syringe. The reaction was allowed to warm to room temperature within 3 h and then the clear solution was transferred via cannula into a flask containing 2.66 g (8.00 mmol) of Cp^*ZrCl_3 in 250 mL of Et_2O cooled to –78 °C. The mixture was slowly warmed to room temperature and stirred for 12 h whereupon the volatiles were removed in vacuo. The residue was extracted with toluene and filtered through a short pad of Celite to afford a yellow solution, which upon concentration and cooling to –35 °C provided yellow crystals of **2b** (2.49 g, 73% yield). For **2b**: ^1H NMR (400 MHz, benzene- d_6) δ 7.98 (s, 1H), 3.06 (q, $^3J = 7.2$ Hz, 2H), 2.03 (s, 15H), 1.12 (s, 15H), 0.96 (d, $^3J = 7.2$ Hz, 3H). Anal. Calcd for $\text{C}_{17}\text{H}_{30}\text{Cl}_2\text{N}_2\text{Zr}$: C 48.09, H 7.12, N 6.60. Found: C 48.19, H 7.02, N 6.36.

Compound 2c. To a solution of 0.25 g (2.00 mmol) of 1-*tert*-butyl-3-ethylcarbodiimide in 50 mL of Et_2O , cooled to 0 °C, was added 1.02 mL of PhLi (2.0 M in cyclopentane/ Et_2O 7:3 mixture, 2.05 mmol) and the resulting mixture was stirred for 3 h. The clear solution was then transferred via cannula into a flask containing a solution of 0.67 g (2.00 mmol) of Cp^*ZrCl_3 in 40 mL of Et_2O at –78 °C. After addition, the mixture was slowly warmed to room temperature and stirred for 12 h whereupon the volatiles were removed in vacuo. The residue was extracted with toluene and filtered through a short pad of Celite to afford a yellow solution, which upon concentration and cooling to –35 °C provided yellow crystals (0.78 g, 78% yield). For **2c**: ^1H NMR (400 MHz, benzene- d_6) δ 6.93 (d, 2H), 6.88 (m, 3H), 2.91 (q, $J = 7.2$ Hz, 2H, CH_2CH_3), 2.13 (s, 15H, C_5Me_5), 1.15 (s, 9H, CMe_3), 0.87 (t, $J = 7.2$ Hz, 3H, CH_2CH_3). Anal. Calcd for $\text{C}_{23}\text{H}_{34}\text{Cl}_2\text{N}_2\text{Zr}$: C 55.17, H 6.79, N 5.60. Found: C 54.99, H 6.53, N 5.81.

Compound 2d. The same procedure as for **2c** was followed except tBuLi was used in place of PhLi. For **2d**: ^1H NMR (400 MHz, benzene- d_6) δ 3.39 (q, $J = 7.2$ Hz, 2H, CH_2CH_3), 2.04 (s, 15H, C_5Me_5), 1.37 (s, 9H), 1.20 (s, 9H), 1.09 (t, $J = 7.2$ Hz, 3H, CH_2CH_3). Anal. Calcd for $\text{C}_{21}\text{H}_{38}\text{Cl}_2\text{N}_2\text{Zr}$: C 51.04, H 7.76, N 5.55. Found: C 51.23, H 7.77, N 5.43.

$\text{tPrN}=\text{C}(\text{H})\text{-NH}(\text{tPr})\text{SiEt}_3$. A mixture of 10.1 g (80.0 mmol) of 1,3-diisopropylcarbodiimide, 11.1 g (95.4 mmol) of triethylsilane, and 0.24 g (1.35 mmol) of PdCl_2 was sealed in a Schlenk tube and heated at 150 °C overnight. After the mixture was cooled to room temperature, the crude product was vacuum distilled (90 °C (7 mmHg)) to provide a light yellow liquid (12.6

(23) For a recent review, see: Reetz, M. T. *Combinatorial Methods in Catalysis by Metal Complexes*. In *Comprehensive Coordination Chemistry II* **2004**, 9, 509–548.

Table 3. Crystal Structure and Refinement Data for Compounds 1d, 2b–d, 6b, 6d, and 7

parameter	1d	2b	2c	2d	6b	6d	7
empirical formula	C ₄₆ H ₄₁ BF ₂₀ N ₂ Zr	C ₁₇ H ₃₀ Cl ₂ N ₂ Zr	C ₂₃ H ₃₄ Cl ₂ N ₂ Zr	C ₂₁ H ₃₈ Cl ₂ N ₂ Zr	C ₁₉ H ₃₆ N ₂ Zr	C ₂₃ H ₄₄ N ₂ Zr	C ₄₇ H ₃₅ BCl ₁₂ F ₂₀ N ₂ Zr
formula wt	1103.84	424.55	500.64	480.65	383.72	439.82	1180.70
temp (K)	193(2)	203(2)	193(2)	193(2)	203(2)	193(2)	173(2)
wavelength (Å)	0.71073	0.71073	0.71073	0.71073	0.71073	0.71073	0.71073
cryst syst	monoclinic	monoclinic	monoclinic	monoclinic	monoclinic	monoclinic	orthorhombic
space group	P2(1)/n	P2(1)/c	P2(1)/n	P2(1)/c	P2(1)/c	P2(1)/c	Pbca
a (Å)	17.4507(5)	8.4813(2)	12.9186(4)	18.687(3)	10.1924(2)	8.9053(18)	22.4895(5)
b (Å)	32.4226(9)	14.9398(4)	14.0189(4)	18.867(3)	11.7577(3)	9.984(2)	17.4563(4)
c (Å)	18.0794(5)	16.1598(5)	13.7982(4)	14.364(2)	17.2669(4)	28.057(6)	24.1544(6)
α (deg)	90	90	90	90	90	90	90
β (deg)	114.0510(10)	90.2310(10)	102.6380(10)	110.486(2)	102.22	98.507(3)	90
γ (deg)	90	90	90	90	90	90	90
vol (Å ³)	9341.2(5)	2047.57(10)	2438.37(12)	4744.0(12)	2022.37(8)	2467.1(9)	9482.6(4)
Z	8	4	4	8	4	4	8
D _{calc} (g cm ⁻³)	1.570	1.377	1.364	1.346	1.260	1.184	1.654
abs coeff (mm ⁻¹)	0.351	0.797	0.681	0.697	0.544	0.454	0.461
F(000)	4448	880	1040	2016	816	944	4720
θ range (deg)	1.76–25.00	2.40–30.00	1.96–27.50	1.16–27.50	2.41–30.00	2.17–27.50	1.70–25.00
no. of rflns	64759	22800	38861	10852	39415	5555	127959
no. of independent rflns	16440	5952	5600	10852	5888	5567	8357
abs corr	[R(int) = 0.0300] empirical, SADABS	[R(int) = 0.0145] semiempirical from equivalents	[R(int) = 0.0543] empirical, SADABS	[R(int) = 0.0000] empirical, SADABS	[R(int) = 0.0184] empirical, SADABS	[R(int) = 0.0000] empirical, SADABS	[R(int) = 0.0390] empirical, SADABS
refinement method	full-matrix least-squares on F ²	full-matrix least-squares on F ²	full-matrix least-squares on F ²	full-matrix least-squares on F ²	full-matrix least-squares on F ²	full-matrix least-squares on F ²	full-matrix least-squares on F ²
goodness-of-fit	1.092	1.074	1.146	1.075	1.075	1.113	1.079
final R indices [I > 2σ(I)]	R1 = 0.0463, wR2 = 0.1269 [12639 data]	R1 = 0.0233, wR2 = 0.0611 [5347 data]	R1 = 0.0398, wR2 = 0.1103 [4113 data]	R1 = 0.0493, wR2 = 0.1370 [7625 data]	R1 = 0.0197, wR2 = 0.0509 [5424 data]	R1 = 0.0488, wR2 = 0.1291 [5204 data]	R1 = 0.0632, wR2 = 0.1895 [6664 data]
R indices (all data)	R1 = 0.0650 wR2 = 0.1388	R1 = 0.0276 wR2 = 0.0641	R1 = 0.0654 wR2 = 0.1211	R1 = 0.0845 wR2 = 0.1583	R1 = 0.0224 wR2 = 0.0525	R1 = 0.0521 wR2 = 0.1311	R1 = 0.0800 wR2 = 0.2043
largest diff peak and hole (e·Å ⁻³)	2.058 to –0.782	0.532 and –0.555	0.782 and –0.544	1.757 and –1.124	0.568 and –0.286	1.228 and –1.142	0.992 and –1.551

g, 66% yield). ^1H NMR (400 MHz, benzene- d_6 , 25 °C) δ 7.53 (s, 1H), 3.52 (septet, $^3J = 6.8$ Hz, 1H), 3.11 (septet, $^3J = 6.8$ Hz, 1H), 1.26 (d, $^3J = 6.8$ Hz, 1H), 1.26 (d, $^3J = 6.8$ Hz, 6H), 1.05 (d, $^3J = 6.8$ Hz, 6H), 0.92 (t, $^3J = 7.6$ Hz, 9H), 0.71 (q, $^3J = 7.6$ Hz, 6H).

$\text{PrN}=\text{C}(\text{H})\text{-NH}(\text{Pr})$. To 11.6 g (47.8 mmol) of freshly distilled $\text{PrN}=\text{C}(\text{H})\text{-NH}(\text{Pr})\text{SiEt}_3$ was added 1.8 g (56 mmol) of methanol. After 1 h, the crude product was vacuum distilled to provide 5.0 g (81%) of a colorless liquid. ^1H NMR (400 MHz, CDCl_3 , 25 °C) δ 7.35 (s, 1H), 3.42 (septet, $^3J = 6.4$ Hz, 2H), 3.09 (br s, 1H), 1.12 (d, $^3J = 6.4$ Hz, 12H). ^{13}C NMR (100 MHz, CDCl_3 , 25 °C) δ 150.2, 24.9, 7.2, 6.8.

Compound 3. The same procedure as that for **2b** was followed, except $\text{PrN}=\text{CH-NH}(\text{Pr})$ was used instead of $\text{t-BuN}=\text{CH-NH}(\text{Et})$. Yield: 75%. For **3**: ^1H NMR (400 MHz, benzene- d_6) δ 8.14 (s, 1H), 3.46 (septet, $^3J = 6.8$ Hz, 2H), 2.01 (s, 15H), 1.00 (d, $^3J = 6.8$ Hz, 12H). ^{13}C NMR (100 MHz, benzene- d_6 , 25 °C) δ 159.9, 125.4, 50.9, 24.2, 12.4. Anal. Calcd for $\text{C}_{17}\text{H}_{30}\text{Cl}_2\text{N}_2\text{Zr}$: C 48.09, H 7.12, N 6.60. Found: C 48.35, H 7.17, N 6.23.

Compounds 6b–e. To a solution of 0.30 g (0.71 mmol) of **2b** in 20 mL of Et_2O , cooled to -78 °C, was added 1.10 mL (14.3 mmol) of MeLi in Et_2O . The mixture was allowed to warm to room temperature over a period of 1 h and then stirred at this temperature for an additional hour before being quenching by the addition of an excess of chlorotrimethylsilane and the volatiles were removed in vacuo. Extraction of the residue into pentane and filtration through a thin pad of Celite afforded a light-yellow solution, which upon concentration and cooling to -35 °C provided off-white crystals of **6b** (0.19 g, 70%). For **6b**: ^1H NMR (400 MHz, benzene- d_6) δ 8.25 (s, 1H), 2.91 (q, $^3J = 7.2$ Hz, 2H), 1.99 (s, 15H), 1.07 (s, 9H), 0.94 (t, $^3J = 7.2$ Hz, 3H), 0.26 (s, 6H). ^{13}C NMR (100 MHz, benzene- d_6 , 25 °C) 165.2, 120.5, 46.1, 32.1, 23.0, 18.7, 14.9, 12.3. Anal. Calcd for $\text{C}_{19}\text{H}_{36}\text{N}_2\text{Zr}$: C 59.46, H 9.48, N 7.30. Found: C 59.20, H 9.33, N 7.21.

Compounds **6c–e** were prepared in a similar manner from **2c**, **2d**, and **3**, respectively.

For **6c**: 79% yield. ^1H NMR (400 MHz, benzene- d_6) δ 7.10 (d, 2H), 7.01 (m, 3H), 2.68 (q, $J = 7.2$ Hz, 2H, CH_2CH_3), 2.07 (s, 15H, C_5Me_5), 1.06 (s, 9H, CMe_3), 0.81 (t, $J = 7.2$ Hz, 3H, CH_2CH_3), 0.38 (s, 6H, ZrMe_2). Anal. Calcd for $\text{C}_{25}\text{H}_{40}\text{N}_2\text{Zr}$: C 52.9, H 8.79, N 6.09. Found: C 65.20, H 8.62, N 6.14.

For **6d**: 70% yield. ^1H NMR (400 MHz, benzene- d_6) δ 3.18 (q, $J = 7.2$ Hz, 2H, CH_2CH_3), 1.99 (s, 15H, C_5Me_5), 1.35 (s, 3H, CMe_3), 1.25 (s, 9H, CMe_3), 1.05 (t, $J = 7.2$ Hz, 3H, CH_2CH_3), 0.08 (s, 6H, ZrMe_2). ^{13}C {1H} NMR (benzene- d_6) δ 180.1, 119.3, 55.8, 43.7, 40.7, 40.5, 34.4, 31.4, 19.1, 12.1. Anal. Calcd for $\text{C}_{23}\text{H}_{44}\text{N}_2\text{Zr}$: C 62.79, H 10.10, N 6.37. Found: C 62.89, H 10.41, N 6.12.

For **6e**: 75% yield. ^1H NMR (400 MHz, benzene- d_6) δ 8.31 (s, 1H), 3.17 (septet, $^3J = 6.8$ Hz, 2H), 1.98 (s, 15H), 1.01 (d, $^3J = 6.8$ Hz, 12H), 0.24 (s, 6H). ^{13}C NMR (100 MHz, benzene- d_6 , 25 °C) 161.9, 96.8, 49.0, 43.9, 23.1, 9.9. Anal. Calcd for $\text{C}_{19}\text{H}_{36}\text{N}_2\text{Zr}$: C 59.47, H 9.48, N 7.30. Found: C 59.33, H 9.39, N 7.18.

General Procedure for Polymerization of 1-Hexene.

To a solution of 20 mg (25 μmol) of $[\text{PhNHMe}_2][\text{B}(\text{C}_6\text{F}_5)_4]$ in 8 mL of chlorobenzene, cooled to -10 °C, was added all at once a solution of 11.5 mg (25 μmol) of **6c** in 2 mL of chlorobenzene, also cooled to -10 °C. After 5 min, 0.421 g (5.0 mmol) of 1-hexene, precooled to -10 °C, was added all at once and the resulting mixture was allowed to stir for 2 h at -10 °C, after which time it was rapidly quenched by the addition of methanol. The volatiles were removed in vacuo, and the crude material was purified through precipitation of a toluene solution into a large volume of acidic methanol. The final pure poly(1-hexene) (0.37 g, $M_n = 19\,600$, $\text{PDI} = 1.02$) was collected and dried overnight at 60 °C (0.01 mmHg).

Crystallography. The crystal structure and refinement data for compounds **1d**, **2b–d**, **6b**, **6d**, and **7** are presented in Table 3. The crystallographic analysis of compound **6a** has been previously reported.¹⁹ As a general procedure, for **2b**, a colorless block with approximate orthogonal dimensions $0.40 \times 0.38 \times 0.38$ mm³ was placed and optically centered on the Bruker SMART CCD system at -70 °C. The initial unit cell was indexed by using a least-squares analysis of a random set of reflections collected from three series of 0.3° wide ω -scans, 10 s per frame, and 25 frames per series that were well distributed in reciprocal space. Data frames were collected $[\text{Mo K}\alpha]$ with 0.3° wide ω -scans, 14 s per frame, and 606 frames per series. Five complete series were collected at varying φ angles ($\varphi = 0^\circ, 72^\circ, 144^\circ, 216^\circ, 288^\circ$). An additional 200 frames, a repeat of the first series for redundancy and decay purposes, were also collected. The crystal-to-detector distance was 4.356 cm, thus providing a complete sphere of data to $2\theta_{\text{max}} = 60.0^\circ$. A total of 40872 reflections were collected and corrected for Lorentz and polarization effects and absorption, using Blessing's method as incorporated into the program SADABS^{24,25} with 6178 unique data [$R(\text{int}) = 0.0197$].

All crystallographic calculations were performed on a Personal computer (PC) with a Pentium 1.80 GHz processor and 512 MB of extended memory. The SHELXTL²⁶ program package was implemented to determine the probable space group and set up the initial files. System symmetry, systematic absences, and intensity statistics indicated the unique centric monoclinic space group $P2_1/c$ (no. 14). The 40872 data collected were merged based upon identical indices yielding 22800 data [$R(\text{int}) = 0.0152$], which were further merged during least-squares refinement to 5952 unique data [$R(\text{int}) = 0.0145$]. The structure was determined by direct methods with the successful location of the all non-hydrogen atoms using the program XS.²⁷ The structure was refined with XL.²⁸ An additional least-squares difference Fourier cycle was required to locate the hydrogen atoms. All full-occupancy non-hydrogen atoms were refined anisotropically. Disorder was modeled within the main molecule for part of the amidinate ligand and terminal ethyl group. Hydrogen atoms were allowed to refine freely. A centroid, $C(X)$, was calculated for the pentamethylcyclodienyl ligand. The final structure was refined to convergence [$\Delta/\sigma \leq 0.001$] with $R(F) = 2.76\%$, $wR(F^2) = 6.41\%$, $\text{GOF} = 1.074$ for all 5952 unique reflections [$R(F) = 2.33\%$, $wR(F^2) = 6.11\%$ for those 5347 data with $F_o > 4\sigma(F_o)$]. The final difference Fourier map was featureless, indicating that the structure is both correct and complete. The function minimized during the full-matrix least-squares refinement was $\sum w(F_o^2 - F_c^2)$, where $w = 1/[\sigma^2(F_o^2) + (0.0328P)^2 + 0.6232P]$ and $P = (\max(F_o^2, 0) + 2F_c^2)/3$. An empirical correction for extinction was also attempted but found to be negative and therefore not applied.

Acknowledgment. Funding for this work was provided by the NSF (CHE-0092493) for which we are grateful.

Supporting Information Available: Details of the structure determinations and crystallographic data for complexes **1d**, **2b–d**, **3**, **6b**, **6d**, and **7**. This material is available free of charge via the Internet at <http://pubs.acs.org>.

OM049835Z

(24) Blessing, R. H. *Acta Crystallogr.* **1995**, *A51*, 33–38.

(25) Sheldrick, G. M. *SADABS*; Siemens Area Detector Absorption Correction; University of Göttingen: Göttingen, Germany, 1996.

(26) Sheldrick, G. M. *SHELXTL/PC*, Version 5.03; Siemens Analytical X-ray Instruments Inc.: Madison, WI, 1994.

(27) Sheldrick, G. M. *Acta Crystallogr.* **1990**, *A46*, 467–473.

(28) Sheldrick, G. M. *Shelxl93*, Program for the Refinement of Crystal Structures; University of Göttingen: Göttingen, Germany, 1993.